

Cite this: *RSC Adv.*, 2018, 8, 8349

Dual role of Ag nanowires in ZnO quantum dot/Ag nanowire hybrid channel photo thin film transistors†

Weihao Wang, Xinhua Pan, * Xiaoli Peng, Qiaoqi Lu, Fengzhi Wang, Wen Dai, Bin Lu and Zhizhen Ye

High mobility and p-type thin film transistors (TFTs) are in urgent need for high-speed electronic devices. In this work, ZnO quantum dot (QD)/Ag nanowire (NW) channel TFTs were fabricated by a solution processed method. The Ag NWs play the dual role of dopant and providing the charge transfer route, which make the channel p-type and enhance its mobility, respectively. The best sample yields an on/off ratio (I_{on}/I_{off}) of 5.04×10^5 , a threshold voltage (V_T) of 0.73 V, a high field effect mobility (μ_{FE}) of $8.69 \text{ cm}^2 \text{ V}^{-1} \text{ s}^{-1}$, and a subthreshold swing (SS) of 0.41 V dec^{-1} . Owing to the strong ultraviolet (UV) absorption and photo-induced carrier separation ability of ZnO QDs and the fast carrier transport of Ag NWs, the devices acquire a high external quantum efficiency (EQE) and ultra-fast response under 365 nm UV illumination. The UV-modulated ZnO QD/Ag NW hybrid channel photo TFTs have potential for future application in optoelectronic devices, such as photodetectors and photoswitches.

Received 21st November 2017

Accepted 13th February 2018

DOI: 10.1039/c7ra12642e

rsc.li/rsc-advances

Introduction

Thin film transistors (TFTs) based on metal oxide semiconductors are a key constituent for numerous optoelectronic devices such as sensors and displays. High mobility p-type TFTs are in urgent need for complementary metal oxide semiconductor (CMOS) technology. Wide-band gap metal oxide semiconductors, such as zinc oxide (ZnO),¹ zinc-indium-tin oxide (ZITO),² and indium-gallium-zinc oxide (IGZO)³ have been widely studied for TFTs. ZnO, owing to its abundance, low price, and being indium free, has great potential in the application of TFTs. Various dopants, such as H,⁴ Li,⁵ Na,⁶ Ca,⁷ B,⁸ Al,⁹ and Ti¹⁰ have been utilized to acquire better electrical performance. However, most research is focused on n-type TFTs. p-Type TFTs materials are limited to NiO,^{11–13} SnO,^{14–19} and Cu_xO.^{20–23} There is rarely a report about ZnO-based p-type TFTs due to the difficulty of p-type doping in ZnO.

Recent great progress in light emitting diode (LED) attracts the attention in quantum dots (QDs).²⁴ Quantum confinement effect makes QDs be considered as promising material for the optoelectronic devices. Thus, ZnO QDs with the appropriate band gap may be utilized in ultraviolet (UV)-related photo transistors. Compared with RF magnetron sputtering, pulsed

laser deposition, and atomic layer deposition, solution-processed colloid ZnO QDs can be synthesized at low-temperature to fulfill the progressive demands for low-cost devices. For one-dimensional nano-material, nanowires (NWs) have been widely studied due to the transport of carriers confined in one dimension. Recently, Zou²⁵ and Park²⁶ fabricated NWs and nanorods (NRs) thin film transistors and acquired high field effect mobility (μ_{FE}) owing to this property. The μ_{FE} are $110 \text{ cm}^2 \text{ V}^{-1} \text{ s}^{-1}$ for In₂O₃ single NW TFTs and $1.77 \text{ cm}^2 \text{ V}^{-1} \text{ s}^{-1}$ for ZnO NRs TFTs, respectively. The composite material combined with nanoscale components is the foremost scientific research now, which can take full advantage of these constituents. There were some reports about hybrid channel of ZnO and graphene with UV response.^{27–30} Herein, we employ the Ag NWs utilizing its good conductivity to improve hybrid channel mobility. Besides, Ag is doped into ZnO QDs by annealing, which realizes the ZnO based p-type TFTs. With strong light absorption and photo-induced carriers separation ability of ZnO QDs and fast carrier transport of Ag NWs, it is expected to fabricate these hybrid channel TFTs for the future photo-modulate transistors.

Experimental

Synthesis of colloid ZnO QDs

Colloid ZnO QDs were synthesized by the previous method with some modification.²⁴ In a typical reaction, 3 mmol zinc acetate hydrate and 30 mL dimethyl sulphoxide (DMSO) are loaded in a flask with magnetic stirring under ambient conditions. After zinc acetate being completely dissolved, 10 mL ethanol solution

State Key Laboratory of Silicon Materials, Cyrus Tang Center for Sensor Materials and Applications, School of Materials Science and Engineering, Zhejiang University, Hangzhou 310027, People's Republic of China. E-mail: panxinhua@zju.edu.cn; Fax: +86 571 87952124; Tel: +86 571 87952187

† Electronic supplementary information (ESI) available. See DOI: 10.1039/c7ra12642e



of 5.5 mmol tetramethylammonium hydroxide (TMAH) is added slowly. The reaction is proceeded for 2 h. The obtained stock was divided into 8 parts. Each part is precipitated by adding 5 mL ethyl acetate. After centrifugation, each one is redispersed in 2 mL ethanol with additional ligands of 30 μL 2-ethanolamine to stabilize the nanoparticles. The ZnO QDs are further washed with ethyl acetate and redispersed in 4 mL ethanol. The solution is filtered by 0.22 μL PTFE filter before use. The details of characterization of ZnO QDs are presented in the electronic ESI.†

Devices fabrication

Fig. 1a shows the fabrication process and framework of device. The channel is deposited on the p^{++} Si/300 nm SiO_2 of (100) orientation substrate. The wafers were purchased from University Wafer and cleaned in ultrasonic baths of acetone, ethanol and deionized water for 10 min, respectively, followed by drying with N_2 gas and oxide plasma treatment before used. Then, the Ag NWs film is grown by dip-coating technic. Ag NWs dispersed in ethanol were purchased from Jinan Shangke New Material Co., Ltd. The average length and width of Ag NWs are 60 μm and 80 nm, respectively. The concentration of Ag NWs is diluted to 0.1 mg mL^{-1} and the lifting speed of substrate is 10 $\mu\text{m s}^{-1}$. The NWs would self-assemble aligned owing to the surface tension and solvent evaporation. ZnO QDs were then spin-coated on the NWs film at 3000 rpm. for 35 s, twice. Subsequently, ambient annealing process at different temperature was carried out for 1 h. 100 nm thick Al electrodes were finally evaporated by electron beam evaporation technology with shadow mask as source and drain. The channel width and length were 1000 and 200 μm , respectively.

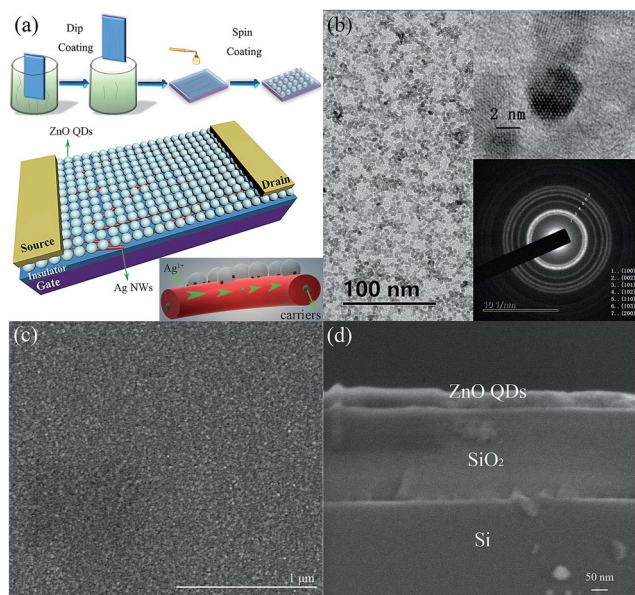


Fig. 1 (a) The schematic diagram of the TFT structure. (b) TEM image and HRTEM image of the ZnO QDs. (c) The surface SEM image of TFT. (d) The cross-section SEM image of TFT.

Characterization

Size and morphologies of ZnO QDs were characterized by high-resolution transmission electron microscopy (HRTEM, JEM-2100). The arrangement of Ag NWs, surface morphologies and cross-section of ZnO QDs film were observed by field-emission scanning electron microscopy (FE-SEM Hitachi S-4800). X-ray photoelectron spectroscopy with a monochromatic Al-K α (1486.6 eV) X-ray source (XPS, Thermo ESCALAB 250) measurements were performed to investigate whether Ag was doped into ZnO QDs after annealing. The performances of TFTs were tested with a semiconductor parameter analyzer (Agilent E5270B). The temporal response of UV was examined with a UVA-LED (365 nm).

Results and discussion

Characterization of hybrid channel

Fig. 1b shows the TEM image of ZnO QDs, and the inserts are HRTEM images. The diameters of ZnO QDs are 4 nm on average. The diffraction rings correspond to the X-ray diffraction (XRD) pattern in the Fig. S2 in the ESI,† which confirms the formation of ZnO phase. Fig. 1c and d are the surface and cross-section SEM images of TFT, respectively. Fig. 1c indicates that the spin-coated ZnO QDs film on the Ag NWs is smooth and flat. And the ZnO QDs film has a thickness of about 50 nm as shown in Fig. 1d.

To investigate the performance of TFTs and reveal the carrier transport of different morphological feature of Ag NWs, the TFTs are annealed at 100, 150, 200, and 300 $^{\circ}\text{C}$, respectively. From Fig. 2, Ag NWs keep the NW shape under 100 and 150 $^{\circ}\text{C}$, while melt into particles under 200 and 300 $^{\circ}\text{C}$. However, ZnO QDs barely have change from the SEM images (the insert graph in Fig. 2).

To clarify whether Ag was doped into ZnO QDs, XPS measurement was conducted on the sample annealed at 100 $^{\circ}\text{C}$.

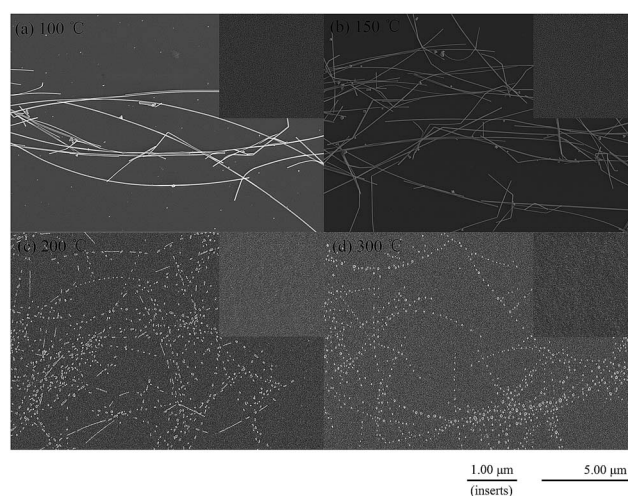


Fig. 2 The SEM images of Ag NWs at different annealing temperature (a) 100 $^{\circ}\text{C}$, (b) 150 $^{\circ}\text{C}$, (c) 200 $^{\circ}\text{C}$, (d) 300 $^{\circ}\text{C}$. Inserts are the corresponding surface of ZnO QDs film.

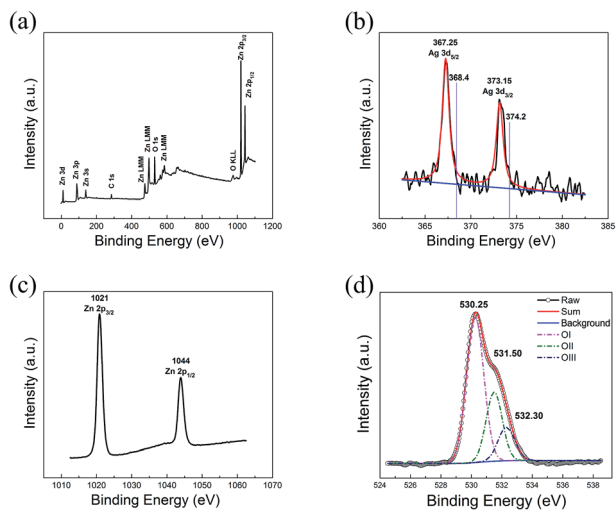


Fig. 3 (a) Complete XPS spectrum of ZnO QDs/Ag NWs hybrid channel annealed at 100 °C. High-resolution spectra of the sample for the elements of (b) Ag, (c) Zn, and (d) O.

Fig. 3a depicts the full spectrum of the sample. C 1s at $E_b = 284.8$ eV is used to the calibration element from the XPS instrument itself. Considering that Ag peak can be hardly observed from full spectrum, high-resolution spectra of Ag, Zn and O are shown in the Fig. 3b–d, respectively. In Fig. 3b, the peaks at binding energy of 367.25 eV and 373.15 eV ascribe to Ag 3d_{5/2} and 3d_{3/2} belonging to the monovalent Ag. There is no zerovalent Ag peak for bulk Ag (368.2 eV of 3d_{5/2} and 374.2 eV of 3d_{3/2}),³¹ which illustrates that the XPS measurements did not observe the Ag NWs. Due to the contact of Ag NWs and ZnO QDs, the Fermi levels of two components equilibrate. Some of the free electrons of Ag NWs transfer to the vacant conduction band (CB) of ZnO QDs at the interfaces of ZnO/Ag, resulting in the monovalent Ag and the p-type ZnO QDs thin film. The peaks centered at 1021 and 1044 eV in the Fig. 3c are attributed to the Zn 2p_{3/2} and 2p_{1/2}, which confirms that Zn exists in divalent states. In Fig. 3d, the O 1s profile can be fitted into three Gaussian distributions representing the different oxygen state. The OI, OII, and OIII belong to the lattice oxygen, oxygen vacancy, and oxygen bonds in the hydroxide, which located at 530.25 eV, 531.50 eV and 532.30 eV, respectively.³²

Devices performance

Fig. 4 shows the transfer characteristics of 4 samples of different annealing temperature under dark and 365 nm UV illumination. As Ag doped into ZnO QDs film investigated by XPS measurements, Fig. 4a–d show p-type transfer characteristic. The electrical parameters, threshold voltage (V_T), μ_{FE} and subthreshold swing (SS), are also listed in each figure. The μ_{FE} is calculated by the following eqn (1):

$$I_{DS}^{1/2} = \sqrt{\frac{W}{2L} C_i \mu_{FE} (V_{GS} - V_T)}, \quad V_{DS} \geq V_{GS} - V_T \quad (1)$$

where I_{DS} , V_{GS} , V_{DS} and C_i are the drain–source current, gate–source voltage, drain–source voltage and the capacitance per

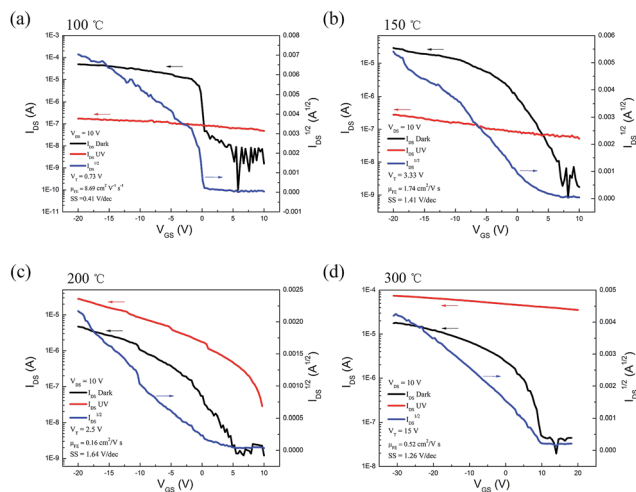


Fig. 4 The transfer characteristics of TFTs under dark and UV illumination at different annealing temperature (a) 100 °C, (b) 150 °C, (c) 200 °C, (d) 300 °C.

unit area of the gate insulator ($0.0115 \mu\text{F cm}^{-2}$), respectively. The SS, another key parameter to indicate the interface defects, is calculated by the eqn (2):

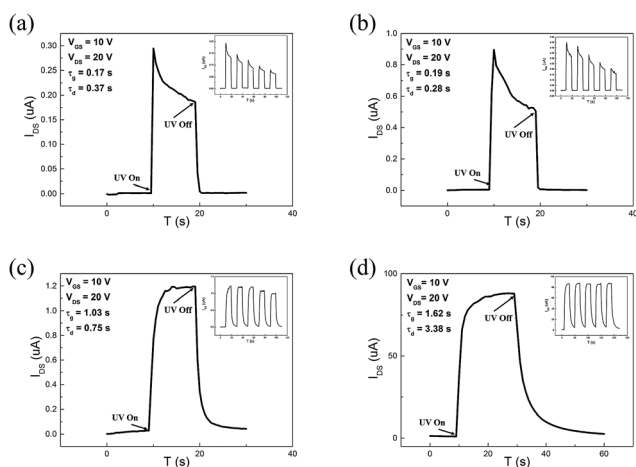
$$SS = \frac{dV_{GS}}{d(\log I_{DS})} \quad (2)$$

It is observed that the performances of devices annealed at 100 and 150 °C are obviously superior to those at higher annealing temperature. As shown in Fig. 2, the Ag NWs transform to Ag particles under 200 and 300 °C annealing. Due to the existence of Ag NWs, the μ_{FE} of devices annealed at 100 and 150 °C are high. The best sample annealed at 100 °C yields an on/off ratio (I_{on}/I_{off}) of 5.04×10^5 , a V_T of 0.73 V, a μ_{FE} of $8.69 \text{ cm}^2 \text{ V}^{-1} \text{ s}^{-1}$, and a SS of 0.41 V dec^{-1} . When the devices illuminated by the 365 nm ultraviolet of $80 \mu\text{W cm}^{-2}$ intensity (P), the transfer curves change differently. Photo-induced holes and electrons from ZnO QDs enhance the conductivity of channel and break the TFTs switch character. The control by V_{GS} is loose, and I_{DS} is a bit amplified and limited by V_{GS} in the accumulation region and depletion region, respectively. Thus, the curves keep particular slopes. It is deduced that the current goes through the Ag NWs in the NW presence devices, and the current flux is limited by the ultra-thin Ag NWs. While in the NW burnt devices, the current path comes to the wider ZnO QDs film. The changes of transfer characteristic and I_{DS} are like our previous research.³³ Electrical parameters of TFTs are summarized in Table 1. The output characteristics of devices under dark and UV illumination are presented in the Fig. S5 and S6 in the ESI,† and the transfer characteristics of ZnO QDs film without Ag NWs is shown in Fig. S7 in the ESI.†

To further reveal the charge transport route, time-resolved UV photocurrent on/off measurements are carried out, as shown in Fig. 5. The inserts are five repeated cycles. V_{GS} was set at 10 V to confine the current at dark (I_{dark}). It can be clearly seen from Fig. 5, the response of 365 nm UV of samples annealed at 100 and 150 °C is much faster than the samples annealed at

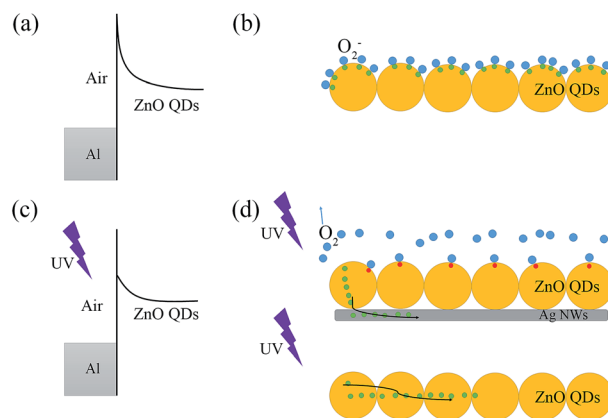
Table 1 Electrical parameters of TFTs with ZnO QDs/Ag NWs hybrid channel

Sample (at different annealing temp.)	V_T (V)	μ_{FE} ($\text{cm}^2 \text{V}^{-1} \text{s}^{-1}$)	SS (V dec^{-1})	I_{on}/I_{off} ($\times 10^5$)
100 °C	0.73	8.69	0.41	5.04
150 °C	3.33	1.74	1.41	0.36
200 °C	2.5	0.16	1.64	0.39
300 °C	15	0.52	1.26	0.09

**Fig. 5** The growth and decay of photocurrent of photo transistors at different annealing temperature (a) 100 °C, (b) 150 °C, (c) 200 °C, (d) 300 °C. Inserts are five repeated cycles.

200 and 300 °C. The characteristic times for growth (τ_g) and decay (τ_d) of the photocurrent are 0.17 and 0.37 s of sample annealed at 100 °C. In Fig. 5a and b, the photo current (I_{photo}) generates and rapidly soars to a maximum, while exposed to the ultraviolet. Due to the current crowding effect, the carriers accumulate in the NWs and I_{photo} will decrease to a stable value. When the UV light is off, the I_{photo} quenches to I_{dark} level. The response of UV is like our previous ZnO NR UV photodetectors.^{34–36} About samples annealed at 200 and 300 °C, the response is much slow and similar to the ZnO nanoparticles UV photodetector.³⁷ The time-resolved UV response confirms the charge transfer mechanism discussed above.

Fig. 6 depicts the energy band of surface ZnO QDs and the schematic diagram of charge transfer. As a result of the chemical absorbed O_2 on the surface of ZnO QDs without UV light, the oxygen molecules capture free electrons [$\text{O}_2(\text{g}) + \text{e}^- = \text{O}_2^-(\text{ad})$], which makes the band of ZnO QDs bend upward and create a low conductivity depletion region on the surface. The effect is particularly prominent in oxide semiconductors, especially in nano structures. Under UV illumination with photon energy higher than the semiconductor band gap, photo-induced hole–electron pairs generate. The photo-generated holes react with the chemisorbed oxygen [$\text{h}^+ + \text{O}_2^-(\text{ad}) = \text{O}_2(\text{g})$], resulting in increasing of free carrier concentration in the ZnO QDs and forming the carrier transport route in different situation, as shown in Fig. 6b and d.

**Fig. 6** The energy band of the surface ZnO QDs under (a) dark and (c) UV illumination, and the schematic diagram of the charge transfer under (b) dark and (d) UV illumination. Red dots = holes, and green dots = electrons.

Moreover, some significant UV response parameters are listed in Table 2. The calculated values are all applied at V_{GS} of 10 V and V_{DS} of 20 V. The responsivity (R) is used to indicate the photo-to-current efficiency. It is determined by the eqn (3):

$$R = \frac{I_{\text{photo}} - I_{\text{dark}}}{PS}, \quad S = L \times W \quad (3)$$

where P is the optical signal power density, and S is the effective photo-electric conversion area, respectively. The device performance can be expressed in terms of another vital parameter, external quantum efficiency (EQE), which is a function of photon flux density and incident photon energy as eqn (4):

$$\text{EQE} = \frac{I_{\text{photo}}/q}{P/h\nu} \quad (4)$$

where q is the quantity of one electron, h is the Plank constant, and ν is the frequency of absorbed photon. Note that the R and EQE both increase mainly by the I_{photo} in the same condition.

As discussed in XPS data, as-implanted Ag atoms by annealing occupy almost ideal substitutional Zn sites.³⁸ Ag atoms are incorporated in the form of point defects of Ag_{Zn} acceptor in $3d^{10}$ states, with part of the silver formed with silver oxide.³⁹ The Ag_{Zn} acceptor actualizes the formation of p-type ZnO. Besides, the heterojunction formed by ZnO QDs and Ag NWs makes the fast response of UV detection. The photo-induced carriers from UV illuminated ZnO are transferred to Ag NWs and transported away rapidly. The dual role of Ag NWs is depicted clearly in Fig. 1a.

Table 2 UV response parameters of ZnO QDs/Ag NWs hybrid channel TFTs

Sample (at different annealing temp.)	τ_g (s)	τ_d (s)	R (A W^{-1})	EQE (%)
100 °C	0.17	0.37	0.64	218
150 °C	0.19	0.28	2.33	793
200 °C	1.03	0.75	6.01	2048
300 °C	1.62	3.38	351	119 565

Conclusions

In summary, we have fabricated the photo-modulated p-type TFTs with ZnO QDs/Ag NWs hybrid channel, and cleared the charge transfer in the channel under UV illumination. At low annealing temperature of 100 and 150 °C, the Ag NWs firstly provide the Ag dopant and make the thin channel p-type as XPS measurements and TFTs transfer characteristic demonstrated. Moreover, Ag NWs play a role of charge transfer route, which enhances the μ_{FE} . The sample annealed at 100 °C yields an on/off ratio (I_{on}/I_{off}) of 5.04×10^5 , a V_T of 0.73 V, a μ_{FE} of $8.69 \text{ cm}^2 \text{ V}^{-1} \text{ s}^{-1}$, and a SS of 0.41 V dec^{-1} . In addition, the TFTs show superior response of 365 nm UV illumination due to the surface ZnO QDs. Owing to the strong UV absorption and photo-induced carriers separation ability of ZnO QDs and fast carrier transport of Ag NWs, the devices display the high EQE and ultra-fast response. The sample annealed at 100 °C acquire a 0.17 s of τ_g , 0.37 s of τ_d , 0.64 A W^{-1} of responsivity, and 218% EQE. The UV-modulated ZnO QDs/Ag NWs hybrid channel TFTs have potential for the future application in optoelectronic devices, such as photodetector and photoswitch.

Conflicts of interest

There are no conflicts to declare.

Acknowledgements

This work was supported by National Natural Science Foundation of China under Grant No. 51302244 and 91333203, and Zhejiang Provincial Natural Science Foundation of China under Grant No. LY17E020005.

References

- 1 Y. Y. Lin, C. C. Hsu, M. H. Tseng, J. J. Shyue and F. Y. Tsai, *ACS Appl. Mater. Interfaces*, 2015, 7, 22610–22617.
- 2 Q. J. Jiang, J. G. Lu, J. P. Cheng, X. F. Li, R. J. Sun, L. S. Feng, W. Dai, W. C. Yan and Z. Z. Ye, *Appl. Phys. Lett.*, 2014, 105, 132105.
- 3 K. Nomura, H. Ohta, A. Takagi, T. Kamiya, M. Hirano and H. Hosono, *Nature*, 2004, 432, 488–492.
- 4 A. Abliz, C. W. Huang, J. Wang, L. Xu, L. Liao, X. Xiao, W. W. Wu, Z. Fan, C. Jiang, J. Li, S. Guo, C. Liu and T. Guo, *ACS Appl. Mater. Interfaces*, 2016, 8, 7862–7868.
- 5 S. Y. Park, B. J. Kim, K. Kim, M. S. Kang, K. H. Lim, T. I. Lee, J. M. Myoung, H. K. Baik, J. H. Cho and Y. S. Kim, *Adv. Mater.*, 2012, 24, 834–838.
- 6 K. Kim, S. Y. Park, K.-H. Lim, C. Shin, J.-M. Myoung and Y. S. Kim, *J. Mater. Chem.*, 2012, 22, 23120.
- 7 W. Yu, D. Han, G. Cui, Y. Cong, J. Dong, X. Zhang, X. Zhang, Y. Wang and S. Zhang, *Jpn. J. Appl. Phys.*, 2016, 55, 04EK05.
- 8 S. Gandla, S. R. Gollu, R. Sharma, V. Sarangi and D. Gupta, *Appl. Phys. Lett.*, 2015, 107, 152102.
- 9 T. S. Kang, T. Y. Kim, K. S. Yoon, J. M. Kim, H. S. Im and J. P. Hong, *J. Mater. Chem. C*, 2014, 2, 10209–10216.
- 10 G. Cui, D. Han, W. Yu, P. Shi, Y. Zhang, L. Huang, Y. Cong, X. Zhou, X. Zhang, S. Zhang, X. Zhang and Y. Wang, *Jpn. J. Appl. Phys.*, 2016, 55, 04EK06.
- 11 A. Liu, G. Liu, H. Zhu, B. Shin, E. Fortunato, R. Martins and F. Shan, *Appl. Phys. Lett.*, 2016, 108, 233506.
- 12 T. Lin, X. Li and J. Jang, *Appl. Phys. Lett.*, 2016, 108, 233503.
- 13 J. Jiang, X. Wang, Q. Zhang, J. Li and X. X. Zhang, *Phys. Chem. Chem. Phys.*, 2013, 15, 6875–6878.
- 14 R. F. P. Martins, A. Ahnood, N. Correia, L. M. N. P. Pereira, R. Barros, P. M. C. B. Barquinha, R. Costa, I. M. M. Ferreira, A. Nathan and E. E. M. C. Fortunato, *Adv. Funct. Mater.*, 2013, 23, 2153–2161.
- 15 J. A. Caraveo-Frescas, P. K. Nayak, H. A. Al-Jawhari, D. B. Granato, U. Schwingenschlögl and H. N. Alshareef, *ACS Nano*, 2013, 7, 5160–5167.
- 16 J. A. Caraveo-Frescas, M. A. Khan and H. N. Alshareef, *Sci. Rep.*, 2014, 4, 5243.
- 17 Y. S. Li, J. C. He, S. M. Hsu, C. C. Lee, D. Y. Su, F. Y. Tsai and I. C. Cheng, *IEEE Electron Device Lett.*, 2016, 37, 46–49.
- 18 J. H. Lee, Y. J. Choi, C. Y. Jeong, D. K. Jung, S. Ham and H. I. Kwon, *IEEE Electron Device Lett.*, 2016, 37, 295–298.
- 19 P. C. Chen, Y. H. Wu, Z. W. Zheng, Y. C. Chiu, C. H. Cheng, S. S. Yen, H. H. Hsu and C. Y. Chang, *J. Disp. Technol.*, 2016, 12, 224–227.
- 20 A. Dindar, J. B. Kim, C. Fuentes-Hernandez and B. Kippelen, *Appl. Phys. Lett.*, 2011, 99, 172104.
- 21 Z. Q. Yao, S. L. Liu, L. Zhang, B. He, A. Kumar, X. Jiang, W. J. Zhang and G. Shao, *Appl. Phys. Lett.*, 2012, 101, 042114.
- 22 A. Liu, G. Liu, H. Zhu, H. Song, B. Shin, E. Fortunato, R. Martins and F. Shan, *Adv. Funct. Mater.*, 2015, 25, 7180–7188.
- 23 W. Maeng, S.-H. Lee, J.-D. Kwon, J. Park and J.-S. Park, *Ceram. Int.*, 2016, 42, 5517–5522.
- 24 X. Dai, Z. Zhang, Y. Jin, Y. Niu, H. Cao, X. Liang, L. Chen, J. Wang and X. Peng, *Nature*, 2014, 515, 96–99.
- 25 X. Zou, X. Liu, C. Wang, Y. Jiang, Y. Wang, X. Xiao and L. Liao, *ACS Nano*, 2012, 7, 804–810.
- 26 J. H. Park, J. H. Park, P. Biswas, K. Kwon do, S. W. Han, H. K. Baik and J. M. Myoung, *ACS Appl. Mater. Interfaces*, 2016, 8, 11564–11574.
- 27 W. Guo, S. Xu, Z. Wu, N. Wang, M. M. Loy and S. Du, *Small*, 2013, 9, 3031–3036.
- 28 V. Q. Dang, T. Q. Trung, D. I. Kim, T. Duy le, B. U. Hwang, D. W. Lee, B. Y. Kim, D. Toan le and N. E. Lee, *Small*, 2015, 11, 3054–3065.
- 29 V. Q. Dang, T. Q. Trung, T. Duy le, B. Y. Kim, S. Siddiqui, W. Lee and N. E. Lee, *ACS Appl. Mater. Interfaces*, 2015, 7, 11032–11040.
- 30 D. Shao, J. Gao, P. Chow, H. Sun, G. Xin, P. Sharma, J. Lian, N. A. Koratkar and S. Sawyer, *Nano Lett.*, 2015, 15, 3787–3792.
- 31 L. Duan, B. X. Lin, W. Y. Zhang, S. Zhong and Z. X. Fu, *J. Phys. Chem. C*, 2012, 116, 16182–16190.
- 32 Y. Sun, Y. Jiang, H. Peng, J. Wei, S. Zhang and S. Chen, *Nanoscale*, 2017, 9, 8962–8969.
- 33 W. Wang, X. Pan, W. Dai, Y. Zeng and Z. Ye, *RSC Adv.*, 2016, 6, 32715–32720.

- 34 Y. Zeng, X. Pan, W. Dai, Y. Chen and Z. Ye, *RSC Adv.*, 2015, **5**, 66738–66741.
- 35 Y. Zeng, Z. Ye, B. Lu, W. Dai and X. Pan, *Appl. Phys. A*, 2016, **122**, 296.
- 36 Y. Zeng, X. Pan, B. Lu and Z. Ye, *RSC Adv.*, 2016, **6**, 31316–31322.
- 37 Y. Jin, J. Wang, B. Sun, J. C. Blakesley and N. C. Greenham, *Nano Lett.*, 2008, **8**, 1649–1653.
- 38 U. Wahl, E. Rita, J. G. Correia, T. Agne, E. Alves and J. C. Soares, *Superlattices Microstruct.*, 2006, **39**, 229–237.
- 39 N. Gruzintsev, V. T. Volkov and E. E. Yakimov, *Semiconductors*, 2003, **37**, 259–262.